UWB Ranging Accuracy in High- and Low-Data-Rate Applications

Roberta Cardinali, Luca De Nardis, *Member, IEEE*, Maria-Gabriella Di Benedetto, *Senior Member, IEEE*, and Pierfrancesco Lombardo

***Abstract*—The Cramer–Rao lower bound (CRLB) was determined for different ultra-wideband (UWB) signal formats and, in particular, for the two UWB high-data-rate (HDR) signal formats proposed within the IEEE 802.15.3a Task Group, that is, the impulsive direct-sequence UWB (DS-UWB) and the nonimpulsive multiband orthogonal frequency-division multiplexing (MB-OFDM), and an impulsive time hopping (TH) UWB format close to the format for UWB low data rate (LDR) of the forthcoming IEEE 802.15.4a standard. The analysis was carried out for both ideal and multipath channels under power constraints as set by emission masks. Results obtained for HDR formats showed that DS-UWB has better ranging accuracy than does MB-OFDM, thanks to its potentially larger bandwidth and higher frequency of operation. In addition, the degree of multipath strongly affected ranging accuracy, although differently for DS-UWB versus MB-OFDM. When incorporating a correlation receiver structure as well as an Early Late gate synchronizer in the model, ranging performance proved to be related to features of the synchronization sequence. For specific synchronization sequences, in particular, the best ranging accuracy was obtained with MB-OFDM. In the case of LDR, the study analyzed the effect of pulse shape on CRLB. Results showed that a suboptimal choice of the pulse shape reduces the ranging accuracy achievable by TH-UWB signals.**

***Index Terms*—Cramer–Rao lower bound (CRLB), localization, ranging, ultra-wideband (UWB).**

I. Introduction

THE RELEASE of the first world-wide official ultra-wideband (UWB) emission masks by the U.S. Federal Communication Commission (FCC) in February 2002 [1] opened the way, at least in the U.S., to the development of commercial UWB products. The strong power limitations set by the FCC determined as a natural consequence the application scenarios suitable for UWB communications, that is, either high data rates (HDRs) over short ranges, dealt with by the IEEE 802.15.3a Task Group, or low data rates (LDRs) over medium-to-long ranges, within the IEEE 802.15.4a Task Group.

Different UWB high data rate physical layer (HDR-PHY) submissions to the 802.15.3a Task Group converged into two main proposals: the multiband orthogonal frequency-division multiplexing (MB-OFDM) solution, based on the transmission of continuous OFDM signals combined with frequency hopping (FH) over instantaneous frequency bandwidths of 528 MHz [2], and the direct-sequence (DS) UWB proposal, based on impulse radio transmission of UWB DS-coded pulses [3]. As the main focus targeted HDR, final standard specifications lacked requirements on ranging, while a well-known feature of UWB is to allow accurate distance estimation and potentially enable joint communications and ranging. In any case, both MB-OFDM and DS-UWB adopt bandwidths exceeding 500 MHz for UWB emissions in compliance with the UWB definition given by the FCC and can thus provide, when specified, high ranging accuracy.

The UWB good ranging potential was particularly emphasized for location-aware applications in *ad-hoc* and sensor networks; the introduction of positioning in LDR networks forms the main concern of the recent IEEE 802.15.4a Task Group [4], and impulse radio UWB (IR-UWB) radio was proposed as a possible radio transmission technique [5].

Current literature on ranging in UWB systems is rather limited. Published materials either focus on simulation and measurements of UWB ranging and positioning [6], [7] or on theoretical accuracy of UWB synchronization and ranging for time hopping (TH)-IR UWB signals [8], [9], with no specific application IEEE 802.15.3a/4a signal formats. In particular, in [6], a model for ranging error is proposed based on results of a measurement campaign. Similarly, in [7], statistical characterization of ranging error in both line-of-sight (LOS) and not-line-of-site (NLOS) scenarios is carried out based on a set of measured data. However, both works focus on the generic case of a TH-IR UWB signal and do not consider the IEEE 802.15.3a/4a signal formats. Reference [8] provides a theoretical derivation of the Cramer–Rao lower bound (CRLB) for UWB signals, again for TH-UWB signals. Finally, [9] derives the CRLB for a TH-UWB signal. Here, the focus of the paper is on positioning rather than ranging. No numerical analysis of the CRLB for a TH-UWB signal is provided in the paper, however, and HDR signals are not analyzed.

Our study complements previous literature on UWB ranging by providing a theoretical framework for the analysis of achievable ranging accuracy for both HDR and LDR UWB signals, with specific reference to existing UWB power regulations and UWB IEEE 802.15.3a/4a signal formats.

To this aim, we first derive the CRLB for propagation over an ideal channel. The CRLB defines the lower bound on ranging accuracy as a function of signal bandwidth and energy. Next,

Manuscript received July 27, 2005; revised January 9, 2006. This work was supported in part by the European IP Project N. 511766 LIAISON (LocatIon bAsed servIceS for the enhancement of wOrking enviroNment) and by STMicroelectronics Italy under Contract UWB Ranging and Positioning in Radio Communication Systems. This work was presented in part at the IEEE International Conference on Ultra-Wideband, Zurich, Switzerland, September 2005.

The authors are with the Info-Com Department, University of Rome "La Sapienza," 0184 Rome, Italy (e-mail: r.cardinali@infocom.uniroma1.it; lucadn@newyork.ing.uniroma1.it; dibenedetto@newyork.ing.uniroma1.it; pier@infocom.uniroma1.it).

Digital Object Identifier 10.1109/TMTT.2006.871993

we introduce a real channel model that takes into account multipath as well as frequency selectivity and evaluate its impact on ranging accuracy.

Moving from results of our previous work [10]–[12], we first consider both HDR signal formats (MB-OFDM and DS-UWB) and present a complete analytical derivation of the CRLB for ideal and real channel models and under the constraints imposed by power emission masks. We analyze, in particular, the impact of the number and amplitude of signal replicas introduced by multipath on the CRLB. Second, we derive the CRLB for LDR impulsive UWB signals, based on current definition of the IEEE 802.15.4aTG.

This paper is organized as follows. Section II reviews and sets the notation for determining the theoretical limits. Sections III–VI analyze ranging accuracy for HDR UWB signals with the following outline: Section III presents the signal definition for both 802.15.3a proposals; in Sections IV and V, the CRLB is derived for the impulse versus nonimpulse UWB 802.15.3a proposals, for ideal versus real channels. Section VI analyzes the effect of introducing a correlation receiver and synchronization sequences adopted in the two proposals on ranging accuracy. Section VII addresses the LDR case and defines the TH-IR-UWB signal format. Section VIII determines the ranging accuracy achievable with this last signal format by evaluating the corresponding CRLB. Conclusions are drawn in Section IX.

II. CRLB

The CRLB is well known in estimation theory [13]. It estimates the achievable ranging accuracy which is expressed as the minimum achievable variance of the error σ_t^2 when using an ideal unbiased estimator.

A brief description of how to derive the CRLB and application to UWB signals is presented in this section.

Consider a received signal $r(t) = s(t;\{a_k\}) + w(t)$ obtained as the sum of a signal $s(t;\{a_k\})$, function of time t and of parameters $\{a_k\}$, and of thermal noise $w(t)$. In the following, we will focus on the specific case where the only unknown parameter in the set $\{a_k\}$ is propagation delay between transmitter and receiver τ, while all other parameters and, in particular, signal waveform and transmitted symbol sequence are known at the receiver. For a signal bandwidth B, the power of thermal noise is given by

$$\sigma_w^2 = \frac{FkTB}{2}. \tag{1}$$

The signal at the receiver is sampled at frequency $f_s = 1/T_s = B$. The sequence of useful samples is $s_n = s(nT_s;\{a_k\})$, while noise and received signal samples are $w_n = w(nT_s)$ and $r_n = s_n + w_n$, respectively.

The Cramer–Rao theorem indicates that, for any unbiased estimator, the minimal achievable error variance σ_t^2 is

$$\sigma_t^2 \geq F_n^{-1} \tag{2}$$

where F_n is the Fisher information matrix, defined, in our case, as follows:

$$\begin{aligned} F_n &= -E\left\{\left(\frac{\partial}{\partial\tau}\ln\left(p_s\left(\tau;\{a_k\}\right)\right)\right)^2\right\} \\ &= -E\left\{\left(\frac{\partial^2}{\partial\tau^2}\ln\left(p_s\left(\tau;\{a_k\}\right)\right)\right)\right\} \end{aligned} \tag{3}$$

where $p_s(\tau;\{a_k\})$ is the probability density function (pdf) with respect to parameter τ. After some calculations one obtains that the minimum achievable variance for any unbiased estimator (CRLB) is given by

$$\sigma_t^2 = \frac{1}{F_n} = \frac{N_0}{4\int \dot{s}^2\left(t;\{a_k\}\right)dt} = \frac{1}{2\left(\frac{2E}{N_0}\right)\beta^2} \tag{4}$$

where

$$\beta^2 = \frac{\int \dot{s}^2\left(t;\{a_k\}\right)dt}{\int s^2\left(t;\{a_k\}\right)dt} = -4\pi^2\frac{\int f^2 S^2\left(f;\{a_k\}\right)df}{\int S^2\left(f;\{a_k\}\right)df}. \tag{5}$$

Equation (4) provides a lower bound for the variance of error in the estimation of the propagation delay measured on the direct path between the transmitter and receiver, assuming that this measurement is not affected by multipath.

Equation (5) shows that the maximum theoretical accuracy achievable with UWB signals is obtained by solving the problem

$$\max_{S(f)}\left\{\int f^2 S^2\left(f;\{a_k\}\right)df\right\} \tag{6}$$

with the constraint

$$S^2(f) \leq T\cdot \mathrm{PSD}_{\mathrm{MASK}}(f) \tag{7}$$

where T is the considered transmission time and $\mathrm{PSD}_{\mathrm{MASK}}(f)$ is the power emission mask. The problem in (6) is solved by choosing $S^2(f) = T\cdot\mathrm{PSD}_{\mathrm{MASK}}(f)$, leading thus to a CRLB that is given by

$$\sigma_t^2 = \frac{N_0}{16\pi^2 T\int f^2 \mathrm{PSD}_{\mathrm{MASK}}(f)df}. \tag{8}$$

Equation (8) provides the CRLB for a receiver placed at an infinitesimal distance from transmitter. For a real distance D and a given channel transfer function $H(f;D)$—in the perfect case, $H(f;D)$ is a pure attenuator—the CRLB is given by the equation

$$\sigma_t^2 = \frac{N_0}{16\pi^2 T\int f^2 \left|H(f;D)\right|^2 \mathrm{PSD}_{\mathrm{MASK}}(f)df}. \tag{9}$$

If one defines the function

$$Z(f) = 2\int_0^f \phi^2 \left|H(f;D)\right|^2 \mathrm{PSD}_{\mathrm{MASK}}(\phi)d\phi \qquad (10)$$

then the CRLB can be written as follows:

$$\sigma_t^2 = \frac{N_0}{16\pi^2 T Z(f)}. \qquad (11)$$

Finally, if the considered signal occupies frequencies in the range $[f_L, f_H]$, then the CRLB is given by

$$\sigma_t^2 = \frac{N_0}{16\pi^2 T\left[Z(f_H) - Z(f_L)\right]}. \qquad (12)$$

In the following sections, we will determine the CRLB for both HDR and LDR UWB signal formats by selecting the corresponding $S^2(f)$.

III. HDR UWB Signal Definition

Notations for the two UWB signal formats under discussion within the IEEE 802.15.3a Task Group are given in this section.

A. MB-OFDM

An OFDM modulated signal consists of the parallel transmission of N signals that are modulated at N frequency carriers f_m $(m = 0, \ldots, N-1)$. All subcarriers f_m are equally spaced by Δf. The binary sequence is usually mapped on a quaternary phase-shift keying (QPSK) constellation, and each QPSK symbol $(c_m = a_m + jb_m)$ modulates a different subcarrier f_m.

The frequency carriers used in the 802.15.3a MB-OFDM format [2] fall between 3.1–10.6 GHz, that is, the frequency interval to which the FCC has allocated a transmission power of −41.3 dBm/MHz [1].

In the 802.15.3a MB-OFDM format, the available frequency interval is divided into 13 frequency intervals. Each interval corresponds to one band of the MB-OFDM and is 528 MHz wide. The center frequency of a band and its number are related according to the following rule:

$$\text{Center frequency for band } n_b = \begin{cases} 2904 + 528 \times n_b, & n_b = 1, \ldots, 4 \\ 3168 + 528 \times n_b, & n_b = 5, \ldots, 13 \end{cases} \quad (\text{MHz}) \qquad (13)$$

The MB-OFDM proposal foresees two different modes of transmission: a mandatory Mode 1 and an optional Mode 2.

Mode 1 uses three bands of operation: Band 1 (3.168 GHz, 3.696 GHz), Band 2 (3.696 GHz, 4.224 GHz), and Band 3 (4.224 GHz, 4.752 GHz).

Mode 2 considers seven bands: Bands 1, 2, 3 (same as Mode 1), Band 6 (6.072 GHz, 6.60 GHz), Band 7 (6.60 GHz, 7.128 GHz), Band 8 (7.128 GHz, 7.656 GHz), and Band 9 (7.656 GHz, 8.184 GHz). The four unmentioned bands have been reserved for future use. Table I contains particularly relevant parameters of the MB-OFDM proposal, such as the number of subcarriers, the duration of the waveform, and the period of the fast Fourier transform (FFT). Additional parameters include a guard interval, introduced for mitigating intersymbol interference (ISI), and the number of pilot carriers, which are used for channel estimation.

TABLE I
Main Parameters of the MB-OFDM Proposal

Parameter	Value
N_{SD}: Number of data sub-carriers	100
N_{SDP}: Number of pilot sub-carriers	12
N_{SG}: Number of guard carriers	10
N_{ST}: Total number of sub-carriers	122 (=N_{SD}+N_{SDP}+N_{SG})
Δf: Sub-carrier frequency spacing	4.125 MHz (=528MHz/128)
T_{FFT}: IFFT/FFT period	242.42 ns (1/ Δf)
T_{CP}: Cyclic prefix duration	60.61 ns (=32/528MHz)
T_{GI}: Guard interval duration	9.47 ns (=5/528MHz)
T_{SYM}: Symbol interval	312.5 ns (=T_{CP}+T_{FFT}+T_{GI})

Symbol duration T_{SYM} is divided into three parts: the useful signal ($T_{\mathrm{FFT}} = 242.4$ ns), the cyclic prefix ($T_{\mathrm{CP}} = 60.61$ ns), and the guard interval ($T_{\mathrm{GI}} = 9.47$ ns), for an overall symbol duration ($T_{\mathrm{SYM}} = T_{\mathrm{FFT}} + T_{\mathrm{CP}} + T_{\mathrm{GI}} = 312.5$ ns). The cyclic prefix, located at the onset of the transmitted signal, is a replica of the final interval of the transmitted signal and is used for synchronization and for channel estimation.

The transmitted signal can thus be written as follows:

$$x(t) = g_T(t) \cdot \sum_{m=0}^{N-1} \left(a_m \cos\left(2\pi(f_p + f_m)t + \phi\right) - b_m \sin\left(2\pi(f_p + f_m)t + \phi\right)\right) \qquad (14)$$

where $g_T(t)$ is the impulse response of the pulse shaper and ϕ is the phase of the carrier at $t = 0$.

B. DS-UWB

A DS-UWB signal consists of a pseudorandomly encoded binary sequence that modulates the amplitudes of a train of short pulses. The bandwidth of such a signal depends on the width of the pulse. The adoption of a pseudorandom sequence guarantees a close to flat power spectral density (PSD).

The transmitter is composed of four main blocks: a repeater, a transmission coder, a pulse amplitude modulation (PAM) modulator, and a pulse shaper.

The repeater introduces redundancy in the transmitted sequence by repeating each bit of the binary input sequence N_s times. The output of the repeater is thus a sequence of $N_s N_b$ bits, where N_b is the number of bits of the input sequence.

The transmission coder applies a binary code of period N_p to the output sequence of the repeater. Most commonly, N_p is a multiple of N_s.

The output sequence of the transmission coder enters the PAM modulator, which generates a train of Dirac pulses located at multiples of T_s.

The output of the PAM modulator enters the pulse-shaper filter with impulse response $p(t)$. The impulse response is a pulse with duration shorter than T_s.

The output signal of the above transmission cascade is expressed as follows:

$$s(t) = \sum_{j=-\infty}^{+\infty} d_j p(t - jT_s) \tag{15}$$

where d_j are the symbols of the output sequence of the PAM modulator.

Similarly to MB-OFDM, the occupied frequencies lie between 3.1–10.6 GHz, where a transmission power of -41.3 dBm/MHz is allocated [1].

The DS-UWB proposal foresees the use of two different carriers located around 4 GHz (low band) and 8 GHz (high band). For the low (high)-frequency band, the filter cutoff frequency (-3-dB point) is about 684 MHz (1368 MHz), leading to a chip duration of 1/57 μs (1/114 μs).

IV. CRLB for HDR Ideal UWB Signal Formats in an Ideal Channel

Here, we consider HDR UWB signals characterized by a PSD that perfectly matches the FCC indoor emission mask within the signal bandwidth; these signals are referred to as ideal signals. The CRLB for such signals can be derived under the hypothesis of an *ideal* channel with transfer function independent of frequency and dependent upon distance between transmitter and receiver D as the inverse of the square of D, i.e.,

$$|H_{\text{ideal}}(f; D)|^2 = \frac{1}{D^2}. \tag{16}$$

From (9), one has

$$\sigma_t^2 = \frac{N_0 D^2}{16\pi^2 T \int f^2 \text{PSD}(f) df}. \tag{17}$$

For a given PSD(f), (17) shows that σ_t^2 depends on D^2 and T, where D is the distance between transmitter and receiver, and T is the observation interval. In terms of distance estimation, it is useful to note that the variance of time estimation error (σ_t^2) is related to the distance estimation error (σ_x^2) in the following way:

$$\sigma_x^2 = c^2 \cdot \sigma_t^2 \tag{18}$$

where c is the propagation speed of the signal.

Fig. 1 plots standard deviation σ_x for the three bands used by MB-OFDM Mode 1 and for the two bands used by DS-UWB as a function of D^2/T.

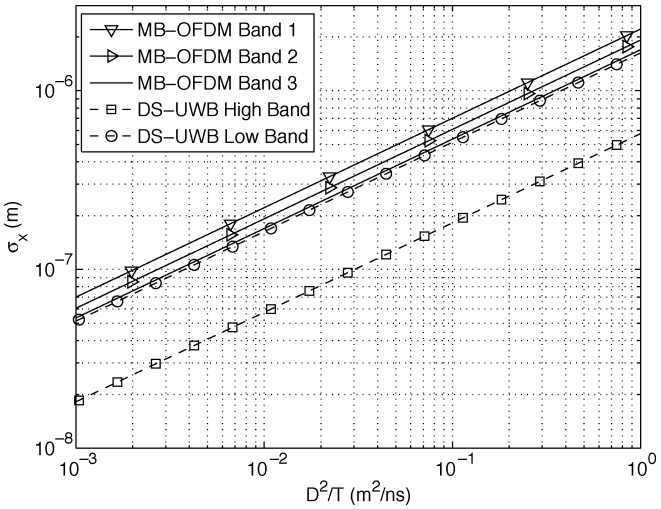

Fig. 1. Standard deviation of distance estimation error σ_x in logarithmic scale for MB-OFDM and DS-UWB HDR signal formats.

Fig. 1 shows that all formats lead to similar trend, but different degrees of accuracy are achievable with different signals due to two factors: the difference in bandwidth and in the center frequency. The high band of DS-UWB has the best ranging performance, thanks to its large bandwidth (1.3 GHz versus 600 MHz of the low band) and its higher frequency carrier. For example, at $D = 1$ m, with an observation time $T = 312.5$ ns, the expected σ_x is about 10^{-7} m. The other formats lead to a ranging error that is almost one degree of magnitude larger, with, as expected, a slightly better performance for Band 3 of MB-OFDM thanks to its higher carrier frequency.

V. CRLB for HDR Real UWB Signal Formats in an Ideal Channel

In the previous section, the standard deviation of the distance estimation error was obtained by using all power available in the power mask. A real signal does not exploit, however, all this power, and in a real signal, the PSD of MB-OFDM and DS-UWB only approximates the FCC mask.

We therefore evaluate CRLB by replacing the FCC power mask for an indoor environment with a real MB-OFDM PSD in the three bands of Mode 1. By substituting $\text{PSD}_{\text{OFDM}}(\phi)$ to PSD(ϕ) in (17), one has

$$\sigma_t^2 = \frac{N_0 D^2}{16\pi^2 T \int f^2 \text{PSD}_{\text{OFDM}}(f) df}. \tag{19}$$

Fig. 2 shows the achievable CRLB values obtained by using a theoretical power mask versus using a real MB-OFDM signal. We can see that differences between ideal and real cases are very small, because the PSD of the MB-OFDM very well approximates power masks.

As for the DS-UWB case, we can evaluate the CRLB by replacing the DS-UWB PSD in (17), yielding

$$\sigma_t^2 = \frac{N_0 D^2}{16\pi^2 T \int f^2 \text{PSD}_{\text{DS}}(f) df}. \tag{20}$$

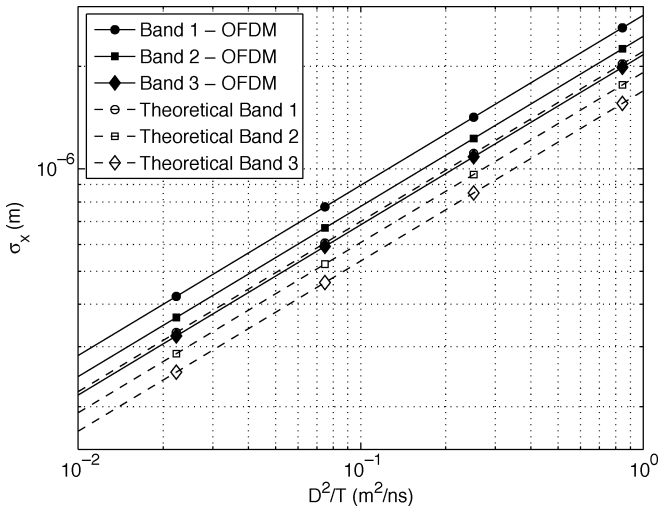

Fig. 2. Standard deviation of distance estimation error σ_x in logarithmic scale for ideal and real MB-OFDM PSD.

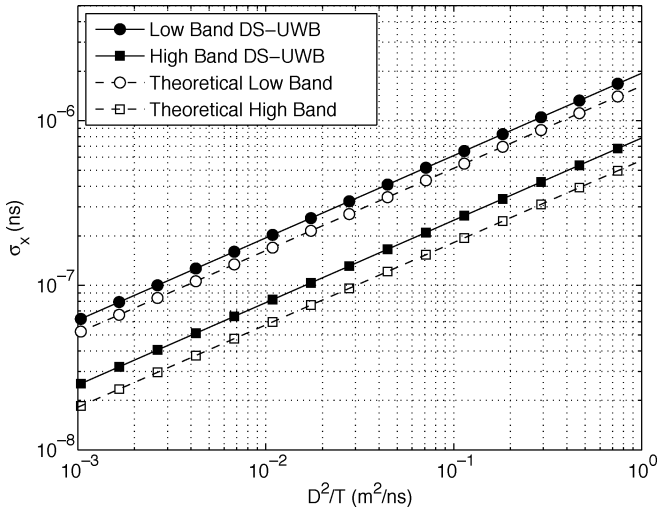

Fig. 3. Standard deviation of distance estimation error σ_x in logarithmic scale for ideal and real DS-UWB PSD.

Fig. 3 shows the CRLB for the ideal versus real DS-UWB case. Similarly to MB-OFDM, the differences between the ideal and real cases are not significant, since the PSD of DS-UWB closely fits the power mask in the area of interest.

VI. CRLB for HDR UWB Signal Formats in a Real Channel

Here, the CRLB is investigated under more realistic conditions of propagation by introducing the channel model proposed within the IEEE 802.15.3a Channel Model subcommittee [2]. This model incorporates a strong multipath, with several overlapped replicas of a transmitted signal. The model assumes that all channel parameters are random variables with specific, well-defined distributions. We can thus consider some realizations of the channel impulse response and evaluate the corresponding CRLB.

TABLE II
Channel Scenarios With Constant Value of τ_0

Scenario Identification	τ_n (ns)	N	k	τ_0 (ns)
A	From 0 to 50 spaced 1 ns	50	0.1	15
B	From 0 to 50 ns spaced 1.25 ns	40	0.1	15
C	From 0 to 50 ns spaced 1.67 ns	30	0.1	15
D	From 0 to 50 ns spaced 2.5 ns	20	0.1	15
E	From 0 to 50 ns spaced 5 ns	10	0.1	15
F	From 0 to 50 ns spaced 50 ns	2	0.1	15

The channel model introduces N replicas of the propagating signal that are equally spaced in time, with amplitudes that depend on both distance and delay. The channel impulse response can be expressed as follows:

$$h(t) = \sum_{n=1}^{N} \alpha_n(D, \tau_n)\delta(t - \tau_n) \tag{21}$$

with

$$\alpha_n(D, \tau_n) = k \cdot \frac{e^{-D}}{D} e^{-\frac{\tau_n}{\tau_0}} \tag{22}$$

where k and τ_0 are constant parameters. In particular, τ_0 influences the amplitude of the replicas due to multipath.

Based on (21) and (22), the channel transfer function can be written as follows:

$$H(f, D) = \sum_{n=1}^{N} \alpha_n(D, \tau_n) e^{j2\pi f \tau_n} \tag{23}$$

leading to the following expression for the CRLB:

$$\sigma_t^2 = \frac{N_0 D^2}{16\pi^2 T \left[Z_0(f_H) - Z_0(f_L)\right]} \cdot \varepsilon^2(f_L, f_H; D) \tag{24}$$

where

$$\varepsilon^2(f_L, f_H; D) = \frac{Z_0(f_H) - Z_0(f_L)}{D^2 \left[Z(f_H) - Z(f_L)\right]}. \tag{25}$$

The term $\varepsilon^2(f_L, f_H; D)$ represents the additional loss due to the presence of a real channel in place of the ideal one.

For the purpose of comparing the two HDR proposals, we refer to a specific set of channel parameters corresponding to the so-called scenario A, as reported in Table II.

Fig. 4 shows CRLB for both the ideal channel and scenario A for MB-OFDM and DS-UWB as a function of D^2/T. Note that, for low distances, losses are contained, while they dramatically increase for higher distances. Note that performance depends

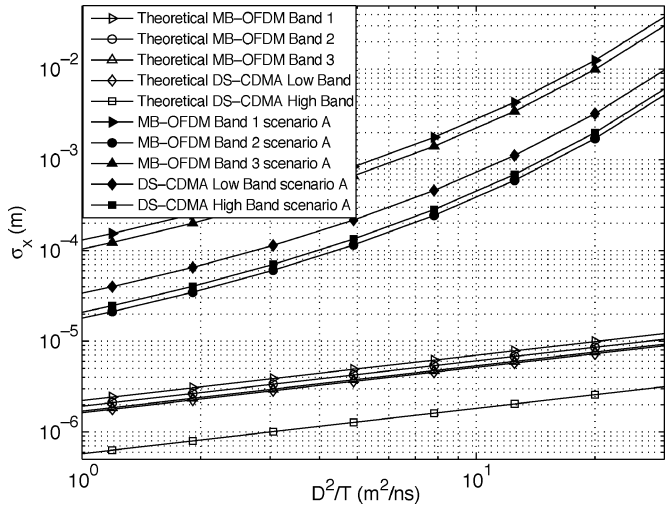

Fig. 4. Standard deviation of distance estimation error σ_x in logarithmic scale for different MB-OFDM and DS-UWB signal formats for an ideal and a non ideal channel (scenario A—see Table II).

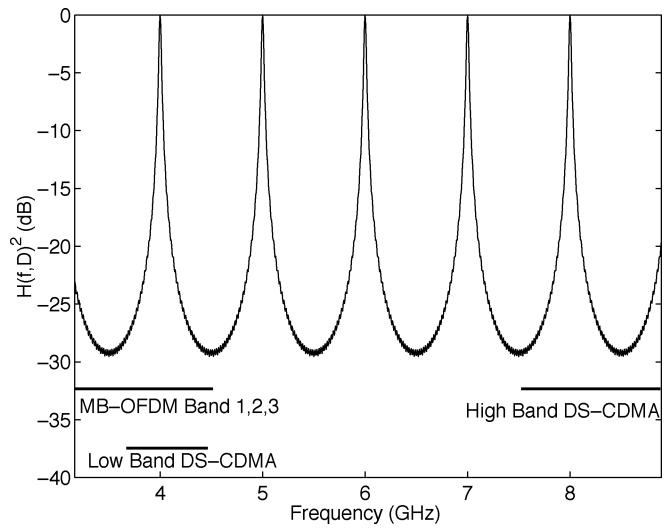

Fig. 5. Modulus of transfer function $|H(f)|^2$ of channel scenario A.

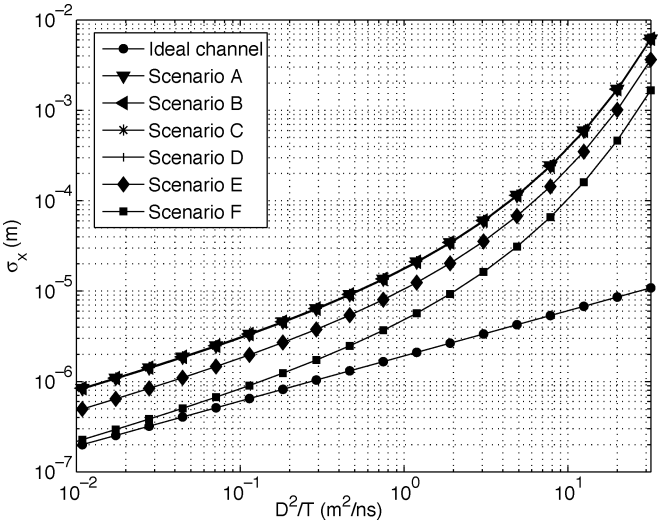

Fig. 6. CRLB obtained for the MB-OFDM signal Band 2 in scenarios defined in Table II

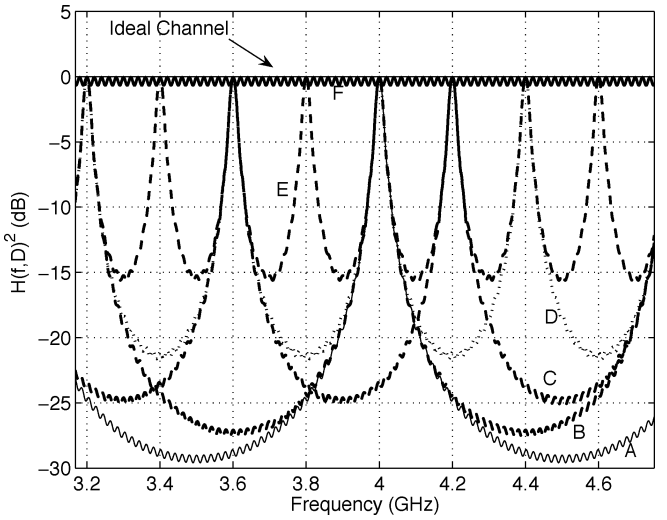

Fig. 7. Modulus of the transfer function of $|H(f)|^2$ for the different channel scenarios as reported in Table II.

exponentially upon distance, since α_n depends on distance as e^{-D}. Fig. 4 shows that, in scenario A, the MB-OFDM in Band 2 leads to the lowest estimation error with a variance of the estimation error that, for low distances, is close to the CRLB achievable with the ideal channel. A similar result is obtained for the DS-UWB formats in both low and high bands.

These results can be explained based on the shape of the transfer function $|H(f)|^2$ of scenario A channel, as shown in Fig. 5. Fig. 5 shows peaks, corresponding to smaller losses, in the frequency ranges corresponding to MB-OFDM Band 2 and to both DS-UWB bands.

Since the channel transfer function depends upon the parameter set, the CRLB also varies as a function of this set.

In order to evaluate the effect of different channel realizations on the corresponding CRLB, we will examine the MB-OFDM Band 2 signal as a test case. The following analysis applies to the DS-UWB case as well.

We will focus in particular on the effect of parameters τ_n, τ_0, and N, which determine the delay between two consecutive replicas, the amplitude of each replica, and the number of replicas, respectively. In order to analyze the impact of τ_n and N, a first set of channel scenarios, reported in Table II, were selected. In this set, k and τ_0 were kept constant, while the values of τ_n and N were selected in order to keep constant the duration of channel impulse response.

Fig. 6 shows the CRLB for MB-OFDM Band 2 in the six above scenarios and in the ideal case of Section V. Note that scenarios with close spacing between replicas (from A to D) lead to a significant increase in CRLB.

Coherently, as the delay between two replicas increases (scenarios E and F), the CRLB approaches the CRLB of an ideal channel.

This effect can be explained by considering the effect of the delay τ_n on the channel transfer function, presented in Fig. 7.

TABLE III
CHANNEL SCENARIOS WITH CONSTANT VALUES OF τ_n AND N

Scenario Identification	τ_n (ns)	N	k	τ_0 (ns)
A1	From 0 to 50 ns spaced 1 ns	50	0.1	31.6228
B1	From 0 to 50 ns spaced 1 ns	50	0.1	12.3548
C1	From 0 to 50 ns spaced 1 ns	50	0.1	4.8270
D1	From 0 to 50 ns spaced 1 ns	50	0.1	1.8859
E1	From 0 to 50 ns spaced 1 ns	50	0.1	0.7368
F1	From 0 to 50 ns spaced 1 ns	50	0.1	0.3162

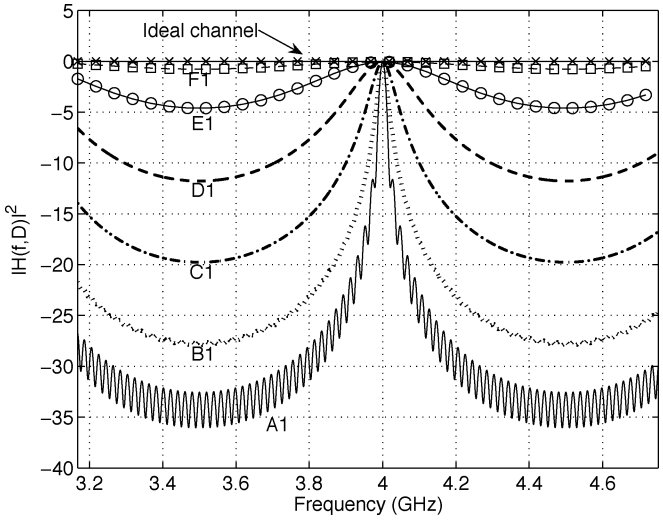

Fig. 8. $|H(f)|^2$ for different channel scenarios as reported in Table III.

Fig. 7 shows in fact that, as τ_n increases, the multipath effect decreases and the channel transfer function tends to resemble the transfer function of an ideal channel. Note that the value of τ_n affects the position and the number of the peaks in the transfer function. The two limit cases are the presence of only two replicas of signal (Scenario F) and the presence of 50 replicas (Scenario A). The transfer function of Scenario F is almost flat, while Scenario A has a significant peak at Band 2 used in the MB-OFDM.

Next, we investigated τ_0 by considering the set of channel scenarios reported in Table III.

Fig. 8 shows channel transfer functions for scenarios of Table III. These functions have a peak at 4 GHz, due to a 1-ns delay between two replicas. Differences among transfer functions are in peak amplitude and width changes with τ_0. For high τ_0, there is a high and narrow peak, while the peak widens and lowers when τ_0 decreases. Gain α_n varies with τ_0 according to an exponential law; when τ_0 decreases, α_n decreases rapidly, leading to a flatter transfer function.

Fig. 9 shows the CRLB obtained for channel scenarios of Table III. Note that, when τ_0 decreases, the performance gap between Band 2 and the other bands decreases, due to a reduction of the peak value of the transfer function.

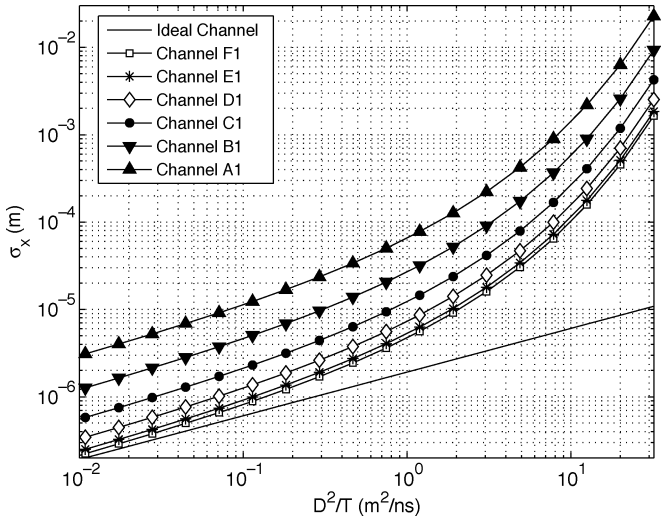

Fig. 9. CRLB obtained for the MB-OFDM Band 2 format in channel scenarios defined in Table III.

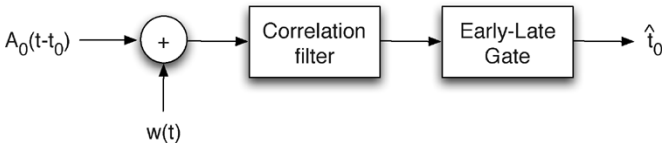

Fig. 10. System model for an Early–Late Gate estimator.

VII. RANGING ACCURACY BASED ON THE USE OF A CORRELATION FILTER

In this section, we introduce the structure of the receiver, composed by a correlation filter with impulse response $p(t)$ combined with a delay lock loop, known as the Early–Late Gate estimator. The receiver structure is presented in Fig. 10, where $s(t)$ is the transmitted signal, $w(t)$ is the additive thermal noise, and A_0 and t_0 are the attenuation and the delay introduced by the channel. The input signal is thus given by $x(t) = A_0 s(t - t_0) + w(t)$.

Under the assumption of $p(t)$ being perfectly matched to $s(t)$, the output of the correlation filter is given by

$$\begin{aligned}\tilde{x}(t) &= x(t) * p(t) \\ &= A_0 \left(s(t-t_0) * p(t)\right) + w(t) * p(t) \\ &= A_0 R_s(t-t_0) + n(t)\end{aligned} \tag{26}$$

where $R_s(t)$ is the autocorrelation of $s(t)$ and $n(t)$ is the filtered noise at the output of the correlator.

The Early–Late Gate provides the maximum-likelihood estimation of the propagation delay by solving the following equation:

$$\frac{\left|\tilde{x}(\hat{t}_0 + \Delta)\right|^2 - \left|\tilde{x}(\hat{t}_0 - \Delta)\right|^2}{2\Delta} = 0 \tag{27}$$

where Δ is the width of the Early–Late Gate and $\hat{t}_0$ is the estimation of the time of arrival. The error of the estimation of the time of arrival is defined as follows:

$$\delta t = \hat{t}_0 - t_0. \tag{28}$$

In order to evaluate the variance of the estimation error defined by (28), we can rewrite (27) as a function of the estimation error. For the first term of the numerator of (27), we have

$$\left|\tilde{x}(\hat{t}_0+\Delta)\right|^2 = A_0^2\left|R_s(\delta t+\Delta)\right|^2 + \left|n(\hat{t}_0+\Delta)\right|^2 + 2A_0\mathrm{Re}\left\{R_s(\delta t+\Delta)n^*(\hat{t}_0+\Delta)\right\}. \tag{29}$$

Since it can be reasonably assumed that both $n(t)$ and δt are small enough to make both the terms $|n(t)|^2$ and $n(t)\delta t$ negligible, (29) can be approximated by means of an expansion in a Taylor series of the first order, leading to

$$\left|\tilde{x}(\hat{t}_0+\Delta)\right|^2 \cong A_0^2\left|R_s(\Delta)\right|^2 + A_0^2\left.\frac{\partial\left|R_s(t)\right|^2}{\partial t}\right|_{t=\Delta}\delta t + 2A_0\left|R_s(\Delta)\right| n'_R(\hat{t}_0+\Delta) \tag{30}$$

where $n_R(t)$ is the real part of noise. By repeating the derivation for the second term of the numerator of (27) and by substituting the approximated expressions in the same equation, we obtain

$$2A_0^2\left.\frac{\partial\left|R_s(t)\right|^2}{\partial t}\right|_{t=\Delta}\delta t + 2A_0\left|R_s(\Delta)\right|\left[n'_R(\hat{t}_0+\Delta) - n'_R(\hat{t}_0-\Delta)\right] = 0 \tag{31}$$

leading to an estimation error given by

$$\begin{aligned}\delta t &= \frac{\left|R_s(\Delta)\right|}{A_0\left.\frac{\partial|R_s(t)|^2}{\partial t}\right|_{t=\Delta}}\left[n'_R(\hat{t}_0-\Delta) - n'_R(\hat{t}_0+\Delta)\right] \\ &= \frac{\left|R_s(\Delta)\right|}{2A_0\left|R_s(\Delta)\right|\left.\frac{\partial|R_s(t)|}{\partial t}\right|_{t=\Delta}}\left[n'_R(\hat{t}_0-\Delta) - n'_R(\hat{t}_0+\Delta)\right] \\ &= \frac{1}{2A_0\left.\frac{\partial|R_s(t)|}{\partial t}\right|_{t=\Delta}}\left[n'_R(\hat{t}_0-\Delta) - n'_R(\hat{t}_0+\Delta)\right].\end{aligned} \tag{32}$$

The variance of the error δt can be obtained by squaring both sides of (32) and taking the expected value

$$\sigma_t^2 = E[\delta t^2] = \frac{E\left\{\left[n'_R(\hat{t}_0-\Delta) - n'_R(\hat{t}_0+\Delta)\right]^2\right\}}{4A_0^2\left(\left.\frac{\partial|R_s(t)|}{\partial t}\right|_{t=\Delta}\right)^2}. \tag{33}$$

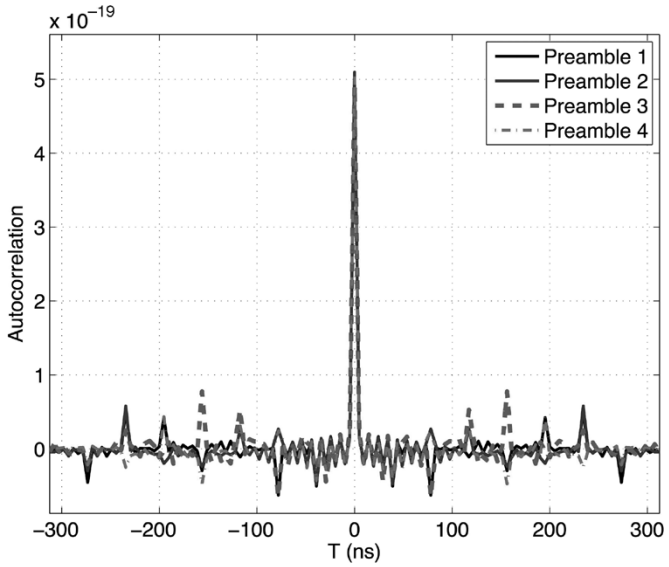

Fig. 11. Autocorrelation functions for the four preambles defined in the MB-OFDM proposal.

Recalling that the noise autocorrelation $R_n(\tau)$ and its real part $R_{n_R}(t)$ satisfy the relation $R_n(t) = 2R_{n_R}(t)$, one has

$$\sigma_t^2 = \frac{\sigma_n^2\left[1-\rho_n(2\Delta)\right]}{4A_0^2\left(\left.\frac{\partial|R_s(t)|}{\partial t}\right|_{t=\Delta}\right)^2} = \frac{1-\rho_n(2\Delta)}{4\mathrm{SNR}\left(\left.\frac{\partial|R_s(t)|}{\partial t}\right|_{t=\Delta}\right)^2} \tag{34}$$

where $\rho_n(\tau) = R_n(\tau)/\sigma_n^2$ is the correlation function of the noise and SNR is the signal-to-noise ratio at the input of the Early–Late gate. In the following, we will use (34) to evaluate the variance of the ranging error.

A. MB-OFDM Synchronization Sequences

The MB-OFDM proposal foresees synchronization performed at each frame and in two phases: acquisition, corresponding to a rough estimation, and tracking that refines the acquisition estimation. Synchronization uses a pilot symbol, known at both transmitter and receiver.

Four different pilot symbols, named preambles, specifically designed to operate in four different environments [2] are defined: preamble 1 for line of sight (LOS) (0–4 m), preamble 2 for not line of sight (NLOS) (0–4 m), preamble 3 for NLOS (4–10 m), and preamble 4 for extreme NLOS.

Fig. 11 shows that the autocorrelations of the four preambles differ in the position and gain of the side lobes.

B. DS-UWB Synchronization Sequences

The DS-UWB proposal foresees three types of preamble for each of the two operation bands. The preambles, referred to as short, medium, and long, are designed for good, nominal, and bad channel scenarios, respectively. We will refer in the following to the medium preamble, since it is the only one available in the proposal description [3].

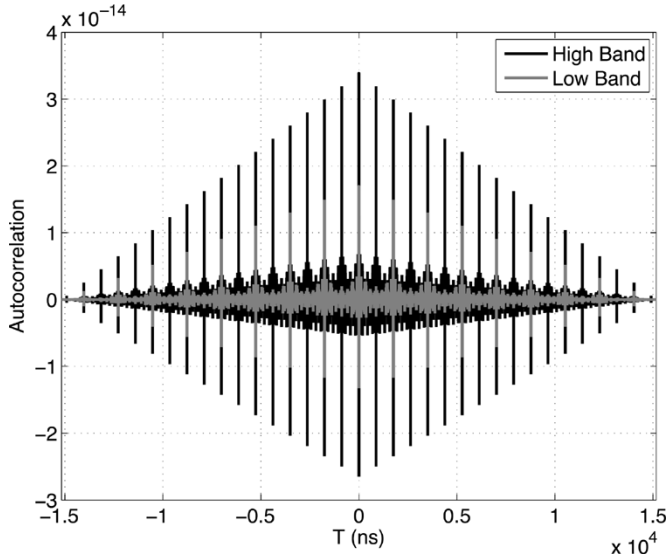

Fig. 12. Autocorrelation functions for the medium preamble case of DS-UWB for low and high bands.

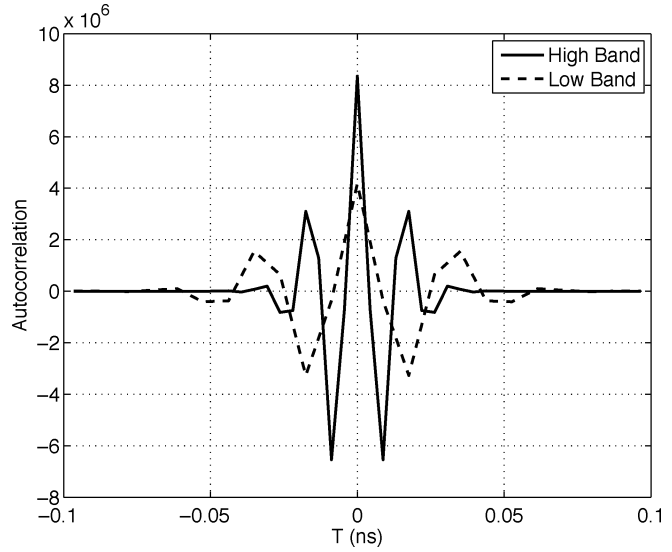

Fig. 13. Zoom of the peak of autocorrelation function of the medium preamble of DS-UWB for low versus high band.

The medium preamble has duration of about 15 μs for both low and high bands. The duration of each bit is about 1/55 μs versus 1/110 μs in low versus high bands, and therefore the number of symbols in the preamble in the high band is twice the number of symbols used in the low band (1730 versus 865).

Fig. 12 shows the autocorrelation functions for the two preambles. As shown, these functions have periodic peaks due to preamble periodicity, allowing synchronization of the receiver with the transmitter. Note in addition the different autocorrelation period for low versus high bands, due to the different symbol rates. Fig. 13 shows a zoom of the autocorrelation and highlights the difference in peak levels.

C. Performance Comparison

Here, we compare accuracy obtained with the correlation filter versus CRLB for an ideal channel.

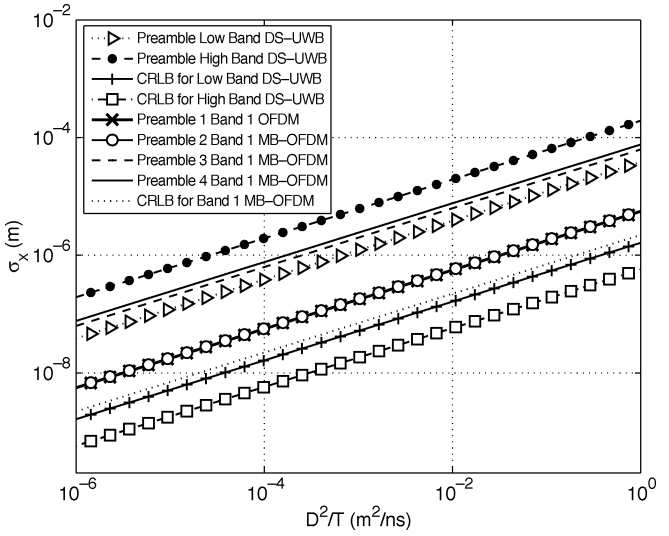

Fig. 14. Comparison of ranging accuracy obtained by using all preambles of the MB-OFDM Band 1 and the medium preambles of DS-UWB for both low and high bands, versus CRLB for MB-OFDM Band 1 and for low- and high-band DS-UWB.

Fig. 14 shows accuracy and CRLB as a function of D^2/T for Mode 1 of MB-OFDM Band 1 and for DS-UWB in both low and high bands. As shown, ranging accuracy with a correlation receiver is about an order of magnitude worse than for CRLB and exhibits similar variation with D^2/T. Under the assumption of ideal channel, SNR decreases in fact as the inverse of D^2, as for CRLB of (17). Fig. 14 also shows the impact of the synchronization sequence on ranging accuracy: preambles 1 and 2 for MB-OFDM lead to better performance than DS-UWB, despite a smaller signal bandwidth. Among MB-OFDM preambles, different accuracy levels due to the different autocorrelations of preambles are observed; preamble 1 leads to the best results, thanks to its narrower autocorrelation, while preambles 3 and 4 lead to the worst performance.

As far as DS-UWB is concerned, note that the characteristics of the high-band preamble lead to the largest ranging error, despite the larger signal bandwidth.

Table IV summarizes the results of the analysis carried out in Sections V–VII.

VIII. TH-IR Signal Format for LDR UWB Networks

A TH-IR UWB signal consists of the transmission of a binary sequence encoded by a pseudorandom sequence that modulates the phase of a train of short pulses. The transmitter is composed of four main blocks: a repeater, a transmission coder, a pulse position modulation (PPM) modulator, and a pulse shaper.

Each bit of the binary sequence is repeated N_s times, so that the output of the repeater is a sequence of N_sN_b bits, where N_b is the number of bits of the input sequence. The repeater thus introduces redundancy in the transmitted sequence. The transmission coder applies a binary code of period N_p to the output sequence of the repeater. Most commonly, N_p is a multiple of N_s.

The output sequence of the transmission coder enters the PPM modulator, which generates a train of Dirac pulses, located at time $kT_s + d_k$, where $\mathbf{d}$ is the output sequence of the transmission coder.

TABLE IV
THEORETICAL RANGING ACCURACY FOR HDR SIGNALS FOR $T = 100$ ns

Signal Format and Channel Scenario	CRLB @ D = 1 m	CRLB @ D = 10 m
DS-UWB Low Band, Ideal Channel	$2*10^{-7}$	$2*10^{-5}$
DS-UWB High Band, Ideal Channel	$5*10^{-8}$	$5*10^{-7}$
MB-OFDM Band 1, Ideal Channel	$2*10^{-7}$	$2*10^{-6}$
DS-UWB Low Band, Multipath Channel, Scenario A	$1.5*10^{-6}$	$3.2*10^{-4}$
DS-UWB High Band, Multipath Channel, Scenario A	$9*10^{-7}$	$2*10^{-5}$
MB-OFDM Band 1, Multipath Channel, Scenario A	$6*10^{-6}$	$1.2*10^{-4}$
DS-UWB Low Band with correlator and medium preamble, Ideal Channel	$4*10^{-6}$	$4*10^{-5}$
DS-UWB High Band with correlator and medium preamble, Ideal Channel	$2*10^{-5}$	$2*10^{-4}$
MB-OFDM Band 1 with correlator and LOS preamble, Ideal Channel	$6*10^{-7}$	$6*10^{-6}$

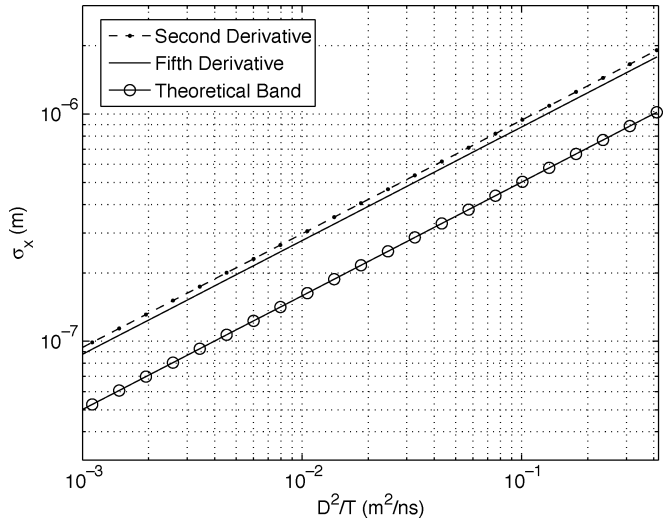

Fig. 15. Standard deviation of distance estimation error in logarithmic scale for a TH-IR UWB signal.

The output of the PPM modulator enters the pulse-shaper filter with impulse response $p(t)$. The impulse response is a pulse with duration shorter than T_s.

The output signal of the transmission cascade is expressed as follows:

$$s(t) = \sum_{j=-\infty}^{+\infty} p(t - jT_s - d_k). \tag{35}$$

IX. CRLB FOR LDR TH-IR UWB SIGNAL FORMATS IN AN IDEAL CHANNEL

Here, the CRLB for LDR TH-IR UWB signals under the hypothesis of an ideal channel is presented. The CRLB expression is reported in (17).

Fig. 15 plots σ_x for the TH-IR UWB signal format as a function of D^2/T, when a bandwidth of about 600 MHz and a frequency carrier of 4.5 GHz is considered, for three different cases: 1) a "theoretical case" where all available bandwidth is used; 2) a first "real case" where the second derivative of the Gaussian function is used as the pulse shaper impulse response; and 3) a second "real case" where the fifth derivative of the Gaussian function is used as the pulse-shaper impulse response.

Note that performance for the "theoretical" PSD is similar to performance for a real TH-IR UWB PSD. Also note that the CRLB obtained with the fifth Gaussian derivative is slightly better than that with the second derivative, since with the fifth derivative the PSD better fits the mask. Since all signals under consideration have the same carrier frequency, this performance difference is mainly due to a different width in the occupied frequencies.

X. CONCLUSION

This paper has investigated the theoretical ranging accuracy obtainable for UWB signal formats proposed within the IEEE 802.15.3a and IEEE 802.15.4a Task Groups regarding HDR and LDR UWB applications, respectively. Our analysis also took into account the emission limits set by the FCC for indoor UWB emissions.

In the case of HDR UWB signals, two signal formats were analyzed: MB-OFDM and DS-UWB. The analysis was carried out by evaluating the CRLB and the standard deviation of distance measurement error for a specific receiver structure. The CRLB was first evaluated under the hypothesis of an ideal channel; results highlighted that DS-UWB using the so-called high band is potentially the best signal format to perform ranging, thanks to its larger bandwidth and higher frequency of operation. Next, the impact of a real channel on ranging accuracy of HDR signals was analyzed by taking into account both temporal spacing and amplitude distribution of signal replicas. Results showed that the presence of multipath strongly affected ranging accuracy for both DS-UWB and MB-OFDM, although to a different extent. Ranging accuracy for HDR systems adopting a correlation receiver followed by an Early–Late Gate was then analyzed, showing that the ranging performance for both signal formats is strictly related to the selected synchronization sequence. As a consequence, the possible advantage of DS-UWB in terms of bandwidth may be compensated by more favorable characteristics of synchronization sequences adopted in the MB-OFDM signal format.

The trend of CRLB for TH-IR UWB signal formats, which are typical of LDR applications, was then analyzed in an ideal channel scenario. Results showed that, although TH-IR signals can potentially achieve a ranging accuracy comparable to that of HDR signals, the selected pulse waveform has, in this case, a significant impact on the distance estimation error, due mainly to bandwidth.

REFERENCES

[1] Federal Communication Commission, Revision of part 15 of the Commission's rules regarding ultra-wideband transmission system: First order and report Tech. Rep. FCC 02-48, Apr. 2002.

[2] A. Batra *et al.*, Multi-band OFDM physical layer proposal for IEEE.802.15 Task Group 3a September 2004 [Online]. Available: http://www.wimedia.org/imwp/idms/popups/pop_download.asp?ContentID=6516

[3] R. Fisher, R. Kohno, H. Ogawa, H. Zhang, K. Takizawa, M. Mc Laughlin, and M. Welborn, DS-UWB physical layer submission to 802.15 Task Group 3a July 2004 [Online]. Available: ftp://ieee:wireless@ftp. 802wirelessworld.com/15/04/15-04-0137-00-003a-merger2-proposal-ds-uwb-update.pdf
[4] IEEE 802.15.TG4a page [Online]. Available: http://www.ieee802.org/15/pub/TG4a.html
[5] M.-G. Di Benedetto and G. Giancola, *Understanding Ultra Wide Band Radio fundamentals*. Upper Saddle River, NJ: Prentice-Hall, 2004.
[6] J. Keignart, N. Daniele, and B. Denis, "Impact of NLOS propagation upon ranging precision in UWB systems," in *Proc. IEEE Conf. Ultra Wideband Syst. Technol.*, Nov. 2003, pp. 379–383.
[7] J.-Y. Lee and R. A. Scholtz, "Ranging in a dense multipath environment using an UWB radio link," *IEEE J. Sel. Areas Commun.*, vol. 20, no. 9, pp. 1677–1683, Dec, 2002.
[8] J. Zhang, R. A. Kennedy, and T. D. Abhayapala, "Cramér–Rao lower bounds for the synchronization of UWB signals," *Eurasip J. Appl. Signal Process.*, vol. 2005, no. 3, pp. 426–438, Mar. 2005.
[9] S. Gezici, Z. Tian, G. V. Giannakis, H. Kobaysahi, A. F. Molisch, H. V. Poor, and Z. Sahinoglu, "Localization via ultra-wideband radios," *IEEE Signal Process. Mag.*, vol. 22, no. 4, pp. 70–84, Jul. 2005.
[10] R. Cardinali, L. De Nardis, P. Lombardo, and M.-G. Di Benedetto, "Theoretical bounds for ranging with multi band OFDM and direct sequence UWB signals," in *Proc. 14th IST Mobile Wireless Commun. Summit*, Dresden, Germany, Jun. 19–23, 2005.
[11] R. Cardinali, L. De Nardis, P. Lombardo, and M.-G. Di Benedetto, "UWB ranging accuracy for applications within IEEE 802.15.3a," in *Proc. Networking With Ultra Wide Band and Workshop on Ultra Wide Band for Sensor Networks*, Rome, Italy, Jul. 2005, pp. 65–69.
[12] R. Cardinali, L. De Nardis, P. Lombardo, and M.-G. Di Benedetto, "Lower bounds for ranging accuracy with multi band OFDM and direct sequence UWB signals," in *Proc. IEEE Int. Conf. UWB*, Zurich, Switzerland, Sep. 2005, pp. 302–307.
[13] H. Urkowitz, *Signal Theory and Random Processes*. Norwell, MA: Artech House, 1983.

Roberta Cardinali received the telecommunication engineering degree from the University of Rome "La Sapienza," Rome, Italy, in 2003, and she is currently working toward the Ph.D. degree at the University of Rome "La Sapienza,"

Her main research topics of interest range from system studies for mono- and bistatic radar to the adaptive signal processing techniques, with particular emphasis on: coherent target detection, clutter modeling, processing techniques for adaptive phased-array antennas. She is currently involved in the design and signal processing for adaptive thinned phased-array antennas and signal processing techniques for GPS and Galileo receivers.

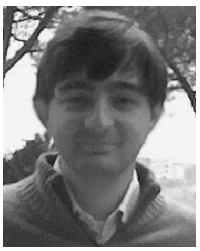

Luca De Nardis (M'98) received the Laurea degree and Ph.D. degree in information and communication theory from the University of Rome "La Sapienza," Rome, Italy, in 2001 and 2005, respectively.

From December 2005 to May 2006, he is a Visiting Scholar with the Electrical Engineering and Computer Science Department, University of California, Berkeley. He is also a Research Affiliate with the University of Rome "La Sapienza." Since 2002, he has been participating in European IST projects focusing on all key aspects of UWB communication systems. He is actually involved in the PULSERS and LIAISON projects dealing with medium access control (MAC), networking, and positioning protocols for UWB networks. His research interests focus on UWB radio technology, *ad-hoc* networks organization, MAC, and routing protocols for wireless networks, and distributed positioning in *ad hoc* and sensor networks.

Maria-Gabriella Di Benedetto (M'01–SM'03) received the Ph.D. degree in telecommunications from the University of Rome "La Sapienza," Rome, Italy, in 1987.

In 1991, she joined the Faculty of Engineering, University of Rome "La Sapienza," where currently she is a Full Professor of telecommunications with the Infocom Department. She has held visiting positions at the Massachusetts Institute of Technology, the University of California, Berkeley, and the University of Paris XI, Paris, France. Her research interests include wireless communication systems and speech science. From 1995 to 2000, she directed four European projects for the design of UMTS. Since 2000, she has been active in fostering the development of UWB radio communications in Europe. Within the 5th framework, she directed for the Infocom Department two European projects (whyless.com and UCAN) aimed at the design and implementation of UWB *ad hoc* networks. Currently, within the 6th EU Framework, her "Networking with UWB" research group participates in the PULSERS Integrated Project which will integrate UWB research and development in Europe for the next several years, and in the LIAISON Integrated Project with regard the application of UWB to location-based services. She also participates in the HYCON network of excellence. She has coedited several special issues on UWB communications and networks for several journals, including the *Journal of Communications and Networks, Mobile Networks and Applications,* and *Eurasip.* She coauthored the first published book on UWB for communications *Understanding Ultra Wide Band Radio Fundamentals* (Prentice-Hall, 2004). She recently completed the coedition of two new books on UWB: *UWB Communication Systems—A Comprehensive Overview* (Hindawi Publishing, 2005), and *Ultra Wideband Wireless Communications* (Wiley, 2005).

Prof. Di Benedetto was the recipient of the Mac Kay Professorship Award from the University of California at Berkeley in 1994.

Pierfrancesco Lombardo received the electronic engineering degree (with distinction) from the University of Rome "La Sapienza," Rome, Italy, in 1991, and the Ph.D. degree in electrical engineering from the University of Rome, Rome, Italy, in 1995.

At the University of Rome, his research focused on detection and estimation techniques for the processing of high-resolution, non-Gaussian SAR images. From 1991 to 1992, he served as an Officer Engineer with the Official Test Center of the Italian Air Force, Pratica di Mare. In 1994, he was a Research Associate with the University of Birmingham, Birmingham, U.K., while working on high-resolution non-Gaussian clutter estimation in the SAR processing team of the Defense Research Agency, Malvern, U.K. He was involved in research on space–time adaptive processing for AEW and SAR at Syracuse University, Syracuse, NY, where he was Research Associate in 1996. In June 1996, he joined the University of Rome "La Sapienza" as a Research Scientist, where he was an Associate Professor from 1998 to 2004 and is presently a Full Professor. He is involved in and coordinates scientific research projects funded by the Italian Space Agency, the Italian Ministry of Research, and the Italian Industry. He leads a group of researchers working at the Radio-positioning Laboratory, University of Rome "La Sapienza" on radar, remote sensing, and navigation. His main interests are in radar adaptive signal processing, radar clutter modeling, radar coherent detection, SAR processing, and radio-localization systems. His research has been reported in over 100 publications in international technical journals and conferences. He has served on the technical committee of many international conferences on radar systems and signal processing.

Dr. Lombardo is a member of the executive team of the IEE Radar Sonar and Navigation Professional Network. He has been an Associate Editor for Radar Systems for the IEEE TRANSACTIONS ON AEROSPACE AND ELECTRONIC SYSTEMS since June 2001. He was chairman of the Technical Committee of the IEEE/ISPRS Joint Workshop on Remote Sensing and Data Fusion over Urban Areas URBAN'2001, Rome, Italy, URBAN'2003, Berlin, Germany, and URBAN'2005, Tempe, AZ. He was the corecipient of the Best Paper Award of the IEEE TRANSACTIONS ON AEROSPACE AND ELECTRONIC SYSTEMS in 2001.